RSC Advances

ROYAL SOCIETY OF CHEMISTRY

www.rsc.org/advances

www.rsc.org/advances

PAPER

Coupling with narrow-band-gap semiconductor for enhancement of visible-light photocatalytic activity: Preparation of Bi_2S_3/g-C_3N_4 and application for degradation of RhB

Xinshan Rong,[a] Fengxian Qiu,[b]* Jie Yan,[b] Hao Zhao,[b] Xiaolu Zhu [b] and Dongya Yang[b]

Received
DOI:

A coupled system for the photodegradation of Rhodamine B dye was realized using Bi_2S_3/g-C_3N_4 composite as a photocatalyst under visible light irradiation. The Bi_2S_3/g-C_3N_4 composite was prepared by a hydrothermal method and characterized by Fourier transform-infrared spectroscopy (FT-IR), X-ray diffraction (XRD), UV-vis diffuse reflectance spectroscopy (DRS), scanning electron microscopy (SEM) and transmission electron microscopy (TEM). Compared with pure g-C_3N_4, Bi_2S_3/g-C_3N_4 sample exhibits an enhanced photocatalytic activity and the best photocatalytic efficiency is 3.68 times more than that of pure g-C_3N_4. The obtained results indicate that coupled system of Bi_2S_3 and g-C_3N_4 could overcome the drawback of low photocatalytic efficiency brought by electron-hole recombination and narrow photoresponse range. On the basis of the corresponding energy band positions, the mechanism of photocatalytic activity enhancement was proposed.

1. Introduction

Recently, semiconductor-based photocatalyst has attracted much attention due to its potential employments in organic and inorganic pollutants remediation in wastewater, and water splitting for hydrogen production.[1, 2] Among numerous semiconductors reported, titanium dioxide (TiO_2) is by far the most popular photocatalyst for its higher photocatalytic activity, good photostability, non-toxicity, and low price.[3] However, the most widely used TiO_2 photocatalyst is only active under UV irradiation (about 4% of solar photons can be used).[4, 5] To effectively eliminate electron-hole recombination in the photocatalytic reaction, many attempts have been made to improve the photocatalytic efficiency. Moreover, upon the viewpoint of utilizing solarlight, developing visible light response photocatalyst is more significant since 45% of the sunlight spectrum is visible light.[6]

Compared with traditional catalyst TiO_2, graphitic-carbon nitride (g-C_3N_4) possesses a proper mid-wide band gap (2.7 eV) to absorb visible light efficiently.[7] Recent years, g-C_3N_4 has drawn much attention for its high photocatalytic performance for degradation ability of organic pollutants under visible light irradiation.[8] Unlike conventional organic semiconductor counterparts, g-C_3N_4 exhibits a unique stability, including the heat endurance and chemical resistance. From reports, the as-prepared g-C_3N_4 is non-volatile up to as high as 600 °C, and will be almost completely decomposed until the temperature rises to 700 °C [9-11] and chemical resistance emerged in that g-C_3N_4 are almost insoluble in water, ethanol, toluene, diethyl ether and tetra hydro furan.[12]The lone pair of nitrogen and electrons delocalization endows the tri-s-triazine derivatives, so g-C_3N_4 with unique electronic structure, which is controllable due to their tunable band gap, and the excellent thermal and chemical stability[13] make it become one of the most promising semiconductor materials in the exciting research field.

According to the above, good performance seems to have endowed g-C_3N_4 a bright future in the application of catalyst. Unfortunately, two main drawbacks of low separation efficiency of photogenerated electron-hole pairs and narrow visible light response range limit its practical application as an efficient visible-light photocatalyst.[14, 15] To improve photocatalytic efficiency, tremendous efforts have been made to improve the efficiency by doping with metal ions or non-metal ions, designing optimizing heterojunctions, and morphological modification. Research by Tian and coworkers showed that the g-C_3N_4/$BiIO_4$ composite photocatalyst displays a higher photocatalytic activity than the two individuals, which can be attributed to its heterojunction structure.[16] Li and coworkers reported that

[a]*School of Environment and Safety Engineering, Jiangsu University, 301 Xuefu Road, Zhenjiang, 212013, P R China*
[b]*School of Chemistry and Chemical Engineering, Jiangsu University, 301 Xuefu Road, Zhenjiang, 212013, P R China. E-mail: fxqiu@ujs.edu.cn; Fax: +86-51188791800; Tel: +86-51188791800*

heterojunctions of graphitic carbon nitride (g-C_3N_4) and Bi_2MoO_6 were synthesized by a hydrothermal method and the heterojunction composites exhibited higher photocatalytic activity than pure g-C_3N_4 or Bi_2MoO_6.[17] Research by Theerthagiri showed that alpha-Fe_2O_3-g-C_3N_4 composite photocatalysts of various compositions by a wet impregnation method and exhibited remarkably improved visible-light induced photocatalytic activity.[18]

To overcome the drawbacks of low photocatalytic efficiency brought by electron-hole recombination and narrow photoresponse range, it was proposed that g-C_3N_4 could be coupled with narrow-band-gap semiconductor for enhancement of visible-light photocatalytic activity. In this study, bismuth sulfide (Bi_2S_3) with a narrow band gap of 1.3 eV was prepared and selected as modifier.[19] The photocatalytic activity evaluation was tested by the degradation of Rhodamine B (RhB) under visible light. The influence of Bi_2S_3 on optical property and the photocatalytic activity of g-C_3N_4 were studied. The influence of time on photocatalytic activity and the reaction kinetics of the composites were also investigated. The obtained results may provide an important indication that how to improve the photocatalytic activity under visible light, not only for g-C_3N_4, but also for the other photocatalyts. As far as we know, a novel Bi_2S_3/g-C_3N_4 composite photocatalyst was designed and used for the degradation of organic pollutants for the first time.

2. Experimental section

2.1 Materials

Dicyandiamide ($C_2H_4N_4$), ethylene glycol ($HOCH_2CH_2OH$, EG), thiourea (NH_2CSNH_2), bismuth nitrate pentahydrate ($Bi(NO_3)_3{\cdot}5H_2O$), nitric acid (HNO_3) and other reagents used in the experiments were obtained from Aladdin Chemical Reagent Co., Ltd. Deionized water was used throughout this study. All chemicals were of analytical grade and were used without further purification.

2.2. Preparation of g-C_3N_4

The graphitic-carbon nitride (g-C_3N_4) samples were prepared by directly heating dicyandiamide.[4] Typically, 2 g of dicyandiamide powder was put into a quartz crucible with a cover, then heated at a rate of 10 ^oC/min to reach a temperature of 600 ^oC; and then tempered at this temperature for 2 h in a flowing-nitrogen atmosphere. After the sample was cooled naturally to room temperature, the resulting powder was grinded in the agate mortar and used in subsequent studies.

2.3. Preparation of photocatalyst

In a typical procedure, 200 mg of g-C_3N_4 was dissolved in 30 mL ethylene glycol under vigorous stirring for 20 min to get the dispersed solution, named solution A. A certain amount of $Bi(NO_3)_3{\cdot}5H_2O$ according to the designed mass ratio of $Bi(NO_3)_3{\cdot}5H_2O$ to g-C_3N_4 was dissolved in diluted nitric acid to form a clear solution. Meanwhile, moderate thiourea was dissolved in 20 mL deionized water. After that, these two solutions were mixed together and the pH of this mixed solution was adjusted to 7 using certain amounts of NaOH solution, which was named solution B. Then, solution A and solution B were mixed together and was stirred for 2 h. The obtained suspension was transferred into a 100 mL teflon-lined stainless steel autoclave up to 80% of the total volume, and then was heated to 160 ^oC and kept at this temperature for 24 h. After being cooled naturally to room temperature, the product was collected and washed using water and ethanol for 3 times, repeatedly, and dried at 60 °C for 12 h. The pure Bi_2S_3 photocatalyst was obtained by the same conditions without adding g-C_3N_4 powder. The process flow chart is illustrated in Scheme 1.

With the above method, a series of Bi_2S_3/g-C_3N_4 composites with various amounts of Bi_2S_3 were prepared according to different mass ratios of $Bi(NO_3)_3{\bullet}5H_2O$ to g-C_3N_4. The final products were named as Bi_2S_3/g-C_3N_4-1, Bi_2S_3/g-C_3N_4-2, Bi_2S_3/g-C_3N_4-3, Bi_2S_3/g-C_3N_4-4 and Bi_2S_3/g-C_3N_4-5 samples, respectively (the mass ratios of $Bi(NO_3)_3{\cdot}5H_2O$ to g-C_3N_4 were 10%, 20%, 30%, 40% and 50%, respectively). In addition, a catalyst with mass ratio of 40% ($Bi(NO_3)_3{\cdot}5H_2O$ to g-C_3N_4) was prepared by a simple mechanical mixing and named as Bi_2S_3&g-C_3N_4-4.

2.4. Characterizations

X-ray diffraction (XRD) patterns of samples were scanned on the Shimadzu LabX-6000 X-ray Diffractometer (40 kV, 30 mA) with a Cu $K\alpha$ radiation source at a scanning rate of 5°/min within the range of 5-90°. Fourier transform-infrared spectra (FT-IR) of all the catalysts (KBr pellets) were recorded on the equipment (AVATAR 360, Madison, Nicolet). UV-vis diffuse reflectance spectroscopy (DRS) was carried out on a Hitachi UV-3010 UV-vis spectrophotometer. $BaSO_4$ was as reference sample. Thermogravimetric analysis (TGA) was performed on a Netzsch STA 449C instrument (NETZSCH Corporation, Germany). The programmed heating range was from room temperature to 800 ^oC at a heating rate of 10 ^oC/min under air atmosphere. The measurement was taken with 6-10mg samples. The size and morphology of the nanoparticles were viewed on a PHI-Tecnai 12 transmission electron microscope (TEM). High resolution transmission electron microscopy (HRTEM) was performed on the FEI-TecnaiG2F30S-Twin transmission electron with a Philips CM200 field-emission gun microscope operating at 197 kV. The photocurrents were measured with an electrochemical analyzer (CHI660B, CHI Shanghai, Inc.). Photoluminescence (PL) spectra of the catalyst were measured on the QuantaMaster^{TM} 40 (Photon Technology International, Inc.).

2.4. Photocatalytic activity

The photocatalytic activity of the photocatalyst was confirmed by the degradation of Rhodamine B (RhB) in an apparatus with a tungsten lamp (500 W) as the irradiation source. The visible-light ($\lambda \geq 420$ nm) used in the present study was obtained by the filter with cut-off wavelength of 420 nm. Photocatalyst (50 mg) was dispersed into 100 mL RhB solution with the concentration of 5 mg/L, and then the mixture was stirred for 30 min in the dark to ensure absorption-desorption equilibrium, after which the reaction suspension was irradiated for 130 min under visible light. The temperature of the suspension was kept at about 25 ^oC by an external cooling jacket with recycled water. The samples were analyzed every 10 min by UV–vis spectrophotometer at maximum absorption characteristic peak of 553 nm (As shown in

Fig. S1, Supplementary Material). A linear calibration curve and correlation coefficient R^2=0.999 are obtained over the range 0 to 5.0 mg/L (as shown in Fig. S2, Supplementary Material). Concentration at time *t* was generally labeled as C. The photocatalytic activity and degradation efficiency were calculated in the form of C/C_0 and $(C_0-C)/C_0$, respectively. Where C_0 (mg/L) is the initial concentration of RhB. *C* (mg/L) is the RhB concentration at time *t* (min).

3. Results and discussion

3.1. Photocatalytic activity comparisons of photocatalysts prepared by mechanical mixing and hydrothermal method

The photocatalytic activity of RhB for blank experiment, Bi_2S_3&g-C_3N_4-4 (Prepared by mechanical mixing method) and Bi_2S_3/g-C_3N_4-4 (Prepared by hydrothermal method) samples were investigated (As shown in Fig. S3, Supplementary Material). From the obtained result, the photocatalytic activity of Bi_2S_3/g-C_3N_4-4 is bigger than that of Bi_2S_3&g-C_3N_4-4. This is mainly because the composition of Bi_2S_3&g-C_3N_4-4, prepared by the physically mixing, is easy to separate and could not form coupled system. So, series of Bi_2S_3/g-C_3N_4 photocatalysts were selected for the further study.

3.2. XRD analysis

X-ray diffraction (XRD) studies were applied to study the phase, crystallinity and structure of the synthesized materials. XRD patterns of g-C_3N_4 (a), Bi_2S_3 (b) and Bi_2S_3/g-C_3N_4-4 (c) samples are shown in Fig. 1. For g-C_3N_4, a strong peak at 2θ = 27.4° marked with square is observed，which was corresponded to the characteristic interplanar staking peak (002) of aromatic systems.[20] For Bi_2S_3/g-C_3N_4-4 sample, the intensity of the peak at 2θ = 27.4° appears an enhancement compared with pure Bi_2S_3, due to the addition of g-C_3N_4. All other prominent peaks at 2θ = 22.19°, 23.57°, 24.95°, 28.58°, 31.72°, 32.97°, 33.85°, 35.73°, 39.96°, 42.72°, 45.48°, 46.61°, 52.53°, 59.15°, 62.55°, 64.89°, 67.60° and 69.31° marked with circle, which were attributed to the (220), (101), (130), (211), (221), (301), (311), (240), (141), (421), (002), (431), (351), (242), (152), (721), (532) and (820) planes of Bi_2S_3, respectively (JCPDS 00-17-0320).[21]

3.3. FT-IR analysis

The chemical structures of g-C_3N_4 and Bi_2S_3/g-C_3N_4 samples were analyzed by FT-IR and the results are shown in Fig. 2, from which it can be seen that the peaks at 1240, 1321, 1408, 1456, 1560 and 1641 cm^{-1} are contributed to the typical stretching modes of CN heterocycles.[22] The absorption peaks near at 1560 and 1641 cm^{-1} are corresponded to C=N stretching, while the peaks observed at 1240, 1321 and 1408 cm^{-1} are attributed to aromatic C–N stretching.[23] The band around 806 cm^{-1} is corresponded to the stretching vibrations of triazine ring.[24] A broad band near 3200 cm^{-1} corresponds to the stretching vibration of O–H of the absorbed water molecule and the stretching modes of terminal NH_2 groups at the defect sites of the aromatic ring.[25] It is worth noting that there were no differences of FT-IR peak between bulk g-C_3N_4 and Bi_2S_3/g-C_3N_4 samples, from which it can be seen that the main characteristic peaks of g-C_3N_4 appeared in all Bi_2S_3/g-C_3N_4 photocatalysts. It is clear that the modification with Bi_2S_3 does not alter the FT-IR absorption bands of the g-C_3N_4 obviously.

3.4. SEM and TEM analysis

To study the morphology of the as-prepared Bi_2S_3/g-C_3N_4 sample, SEM micrographs of pure g-C_3N_4, Bi_2S_3 and Bi_2S_3/g-C_3N_4-4 were taken, as shown in Fig. 3 (a), (b) and (c), respectively. As can be seen from Fig. 3 (a), pure g-C_3N_4 is composed of big irregular particles with a diameter of micron size.[20] The morphology of pure Bi_2S_3 is presented in Fig. 3 (b), showing monodisperse nanorods[26] with a diameter about 70 nm (seen as the inset of Fig. 3 (b)). Fig. 3 (c) shows the SEM morphology of Bi_2S_3/g-C_3N_4-4 composite. Different region exhibits the characteristic morphology of g-C_3N_4, and the similar morphology of Bi_2S_3. The corresponding EDS spectrum and result of Bi_2S_3/g-C_3N_4-4 are displayed in Fig. 3 (d). It can be seen that the Bi_2S_3/g-C_3N_4-4 consists of C, N, Bi and S.

TEM and HRTEM were used to characterize morphology of the samples, and to identify the detailed crystallographic structure and orientation of the Bi_2S_3 nanorod. Fig. 4 (a-c) showed typical TEM of pure g-C_3N_4, Bi_2S_3/g-C_3N_4-4 and amplification of Bi_2S_3/g-C_3N_4-4. Compared with Fig. 4 (a), it can be seen clearly that the TEM of Bi_2S_3/g-C_3N_4-4 is different from that of pure g-C_3N_4. As seen in Fig. 4 (b), the structure of Bi_2S_3 is exhibited as nanorods, which keep consistent with that shown in SEM. Fig. 4 (d) and (e) presented the HRTEM of Bi_2S_3 nanorod, and clear fringe spacing with an interval of 0.36 nm could be indexed to (130) lattice plane of Bi_2S_3 [22]. The crystallographic of Bi_2S_3 is consistent with the result of XRD measurement.

3.5. TG analysis

TGA experiments were carried out on NETZSCH STA449C with the heating rate 10 °C/min under air atmosphere. TG tests of single Bi_2S_3, g-C_3N_4 and all Bi_2S_3/g-C_3N_4 samples were carried out; and TG curves are shown in Fig. 5. The first mass loss process is light from the room temperature to 200 °C, which is originating from the removal of adsorbed O_2 and H_2O. From the curve of pure g-C_3N_4, it can be seen that the g-C_3N_4 is fairly stable when the heat temperature is below 600 °C, and total weight loss is nearly 100% when the temperature is up to 750 °C, which implies that g-C_3N_4 can decompose completely. From the Bi_2S_3 curve, it becomes unstable when the temperature is above 280 °C. This may be due to that Bi_2S_3 can decompose and transform into metal Bi, when the sample was heated about 400 °C. For single Bi_2S_3, the Bi content is calculated with the value of 81.3%. Compared with pure g-C_3N_4, Bi_2S_3/g-C_3N_4 samples become unstable when the temperature is above 280 °C. This is mainly because Bi_2S_3 component was decomposed and transform into metal Bi in the former stage; and g-C_3N_4 component of Bi_2S_3/g-C_3N_4 can decompose completely in the later stage when the temperature is up to 750 °C. The residual mass ratio increases with the increasing addition amount of $Bi(NO_3)_3{\cdot}5H_2O$. For Bi_2S_3/g-C_3N_4-5 sample preparation process, the mass ratio of $Bi(NO_3)_3{\cdot}5H_2O$ to g-C_3N_4 is 50% and the metal Bi content in

Bi_2S_3/g-C_3N_4-5 sample could be easily calculated with the value of 16.99%. As can be seen from Fig. 5 (a, b), the residual mass ratio is about 79.8 and 18.1% when the sample was heated over 750 °C. In consideration of small amount of impurity existing, the test result is according with the theoretical calculation value.

3.6. Optical properties

The UV-vis diffuse reflection spectra (DRS, A and B) of the pure g-C_3N_4 (a), Bi_2S_3/g-C_3N_4-4 (b) and Bi_2S_3 (c) samples are shown in Fig. 6. From Fig. 6 (A), it can be seen that pure g-C_3N_4 has photo-absorption not only in UV light range, but also in visible light range. But the absorption range is relatively narrow, which is less than 500 nm. It is worthy being noted that Bi_2S_3 has strong absorption in nearly the whole range of visible light. Compared with pure g-C_3N_4, the light absorption ability of the composite is significantly enhanced after Bi_2S_3 was introduced, which is attributed to the narrow band gap and large absorption coefficient of Bi_2S_3. As shown in Fig. 6 (B), the proposed band gap of Bi_2S_3/g-C_3N_4-4 shifts to lower energy of 2.3 eV with the addition of Bi_2S_3. The band gap of pure g-C_3N_4 (a) is about 2.7 eV, and which of Bi_2S_3 (c) is about 1.3 eV. The results indicate that the introduction of Bi_2S_3 generated an impurity band and narrowed the band gap of g-C_3N_4.

Furthermore, it is well known that semiconductors with intrinsic band gap structures possess reliable photoelectric properties related to efficient photo-electric conversion. Transient photocurrent responses for the pure g-C_3N_4 (a) and Bi_2S_3/g-C_3N_4-4 (b) were measured to supply an evidence to support that coupling Bi_2S_3 played an important role in the photocatalytic reaction. From the results shown in Fig. 7, it can be seen that the transient photocurrent response of Bi_2S_3/g-C_3N_4-4 (b) is much higher than that of pure g-C_3N_4 (a), which is strong evidence that g-C_3N_4 coupled with Bi_2S_3, the higher efficient separation efficiency of electron-hole pairs would achieve.

Table 1. Degradation efficiency and kinetics parameters for RhB degradation with Bi_2S_3/g-C_3N_4

Sample	RhB degradation efficiency (%)	First-order kinetics	
		Correlation coefficient (R^2)	Apparent kinetic constant (k, min^{-1})
g-C_3N_4	26.61	0.992	0.00259
Bi_2S_3/g-C_3N_4-1	49.29	0.955	0.00571
Bi_2S_3/g-C_3N_4-2	61.45	0.948	0.00833
Bi_2S_3/g-C_3N_4-3	74.69	0.993	0.0111
Bi_2S_3/g-C_3N_4-4	98.10	0.985	0.0310
Bi_2S_3/g-C_3N_4-5	87.40	0.988	0.0148

3.7. Photocatalytic activity measurement

Photocatalytic activity of pure g-C_3N_4 and Bi_2S_3/g-C_3N_4 samples with variable Bi_2S_3 amount were tested by degradation of RhB dye under visible light irradiation and the relative removal of RhB dye molecules in terms of irradiation time were shown in Fig. 8. From the results shown in Fig. 8, direct photolysis of RhB is almost negligible and bare g-C_3N_4 showed a relatively low photocatalytic activity mainly through a photosensitive pathway, while RhB dye degradation efficiency is just 26.61%, as shown in Table 1. Bi_2S_3 displayed a great impact on photocatalytic performance among all samples tested. With the increasing of Bi_2S_3 amount, Bi_2S_3/g-C_3N_4 samples display a dramatically enhancement upon identical conditions. Bi_2S_3/g-C_3N_4-4 has a best photocatalytic activity with the degradation efficiency of 98.10%. However, Bi_2S_3/g-C_3N_4-5 has a relative low photocatalytic activity, compared with Bi_2S_3/g-C_3N_4-4. It is probably because the larger Bi_2S_3 leads to the agglomeration among nanoparticles, and leads to its decreasing photocatalytic activity (As shown in Fig. S4, Supplementary Material). The evolutions of absorption spectra of RhB in the presence of Bi_2S_3/g-C_3N_4-4 under visible irradiation with different time are shown in Fig. S5 (Supplementary Material). It is clearly seen that the characteristic absorption band of RhB solution at 553 nm gradually diminishes in intensity with the increasing irradiation time. Moreover, no new absorption peaks appear, indicating the degradation of RhB and no other organic molecules generating. To clarify the final products after decomposition, the total organic carbon (TOC) values of residual RhB after the photodegradation of 5 mg/L RhB solution over Bi_2S_3/g-C_3N_4-4 were measured (As shown in Fig. S6, Supplementary Material) and are obviously reduced within 130 min. The result indicates that RhB molecules have been decomposed into CO_2 and H_2O.

The experimental data were fitted with a pseudo-first-order model to study reaction kinetics of RhB degradation. As shown in Fig. 9, the corresponding $\ln(C_0/C)$ plot has a good linearity against time, indicating that the visible-light-driven photocatalytic degradation of RhB solutions in the presence of Bi_2S_3/g-C_3N_4 follows the first-order kinetics. From Table 1, all tested samples display a good linearity and possess high correlation coefficient. Bi_2S_3/g-C_3N_4-4 sample shows the largest reaction rate among all Bi_2S_3/g-C_3N_4 samples that is nearly 12.0 times higher than that of pure g-C_3N_4.

3.8. Photocatalytic mechanism of Bi_2S_3/g-C_3N_4 photocatalyst

To improve photogenerated carriers separation and enhance the efficiency of the interfacial charge transfer, one of the most valuable is to use two semiconductors in contact with different redox energy levels of conduction band (CB) and valence band (VB). In this study, g-C_3N_4 was coupled with narrow-band-gap semiconductor (Bi_2S_3) for enhancement of visible-light photocatalytic activity. It is generally accepted that the relative positions of energy bands of g-C_3N_4 (E_{VB} = 1.57 eV, E_{CB} = -1.13 eV)[28] and Bi_2S_3 (E_{VB} = 1.42 eV, E_{CB} = 0.12 eV)[19] are shown in Scheme 2. When the Bi_2S_3/g-C_3N_4 composites are irradiated under visible light, both g-C_3N_4 and Bi_2S_3 can easily absorb visible light and be excited to produce photogenerated electron-

hole pairs. The photogenerated holes (h^+) in VB of g-C_3N_4 and Bi_2S_3 can directly oxidize RhB. The photogenerated electrons (e^-) in CB of g-C_3N_4 and Bi_2S_3 can be captured by oxygen adsorbed on the surface of Bi_2S_3/g-C_3N_4 composites to generate $\bullet O^{2-}$, further to form •OH, which would be responsible for the degradation of RhB.

According to the relative positions of energy bands, the photogenerated holes (h^+) in VB of g-C_3N_4 are easily be transferred to Bi_2S_3. However, the photogenerated electrons in CB of g-C_3N_4 are difficultly injected into Bi_2S_3 because of the potential difference between CB of g-C_3N_4 (−1.13 eV) and Bi_2S_3 (0.12 eV).[29, 30] Due to g-C_3N_4 coupled with Bi_2S_3, h^+ in VB of g-C_3N_4 are easily be transferred to Bi_2S_3, which is the main cause for the efficient separation of the photogenerated electron-hole pairs in g-C_3N_4. Hence, this coupled system effectively reduces the recombination of photoinduced electrons and holes, resulting in enhanced photodegradation efficiency of g-C_3N_4.

The photoluminescence (PL) spectrum is an effective approach to evaluate the separation capacity of the photogenerated charge carriers. In order to prove the effective separation of the photogenerated charges, PL spectra of g-C_3N_4 (a), Bi_2S_3 (b) and Bi_2S_3/g-C_3N_4-4 (c) were shown in Fig. 10. The higher PL intensity means more efficient carriers participate in the recombination. On the contrary, the lower PL intensity means more carriers participate in photocatalytic process. As can be seen from Fig. 10 (a, b), there is a strong emission peak for g-C_3N_4 and a relative low emission peak for Bi_2S_3 at around 482 nm, which could be related to the recombination of the photoexcited electron–hole. However, PL intensity of Bi_2S_3/g-C_3N_4-4 is lower than that of g-C_3N_4 and Bi_2S_3, which suggests the improved charge carrier separation inside the composite.

3.9. Reusability studies

The reusability is an important parameter of the photocatalytic process. In order to examine the photocatalytic stability of the photocatalyst, Bi_2S_3/g-C_3N_4-4 was selected for the recycling experiment and the result is shown in Fig. 11. As can be seen from Fig. 11 (A), the degradation efficiency of RhB is about 96.15% in the fifth run. Therefore, it can be concluded that the photocatalyst has good stability in the experimental conditions. The XRD patterns of Bi_2S_3/g-C_3N_4-4 were examined further to verify durability before and after the photocatalytic reaction. As shown in Fig. 11 (B), the XRD patterns are almost identical, indicating that the sample is stable under light irradiation and has the ability to be reused.

4. Conclusions

In summary, visible-light-driven Bi_2S_3/g-C_3N_4 composites were prepared by a hydrothermal method and studied as photocatalysts for degradation of RhB dye molecules. The photocatalytic activity of the composites increased then decreased with increasing Bi_2S_3 content and Bi_2S_3/g-C_3N_4-4 presents the best photocatalytic efficiency, which is more than 3.68 times that of pure g-C_3N_4. Moreover, from the study of reaction kinetics, it can be seen that Bi_2S_3/g-C_3N_4-4 sample showed the largest reaction rate among all Bi_2S_3/g-C_3N_4 samples which is nearly 12.0 times higher than that of pure g-C_3N_4. On the basis of mechanism discussion, the enhanced activity is attributed to the coupled system which offers a wide response wavelength range and the effective separation of electron-holes pairs. Hence, this study has a guiding significance for the design of coupled system and has potential in environmental remediation applications.

Acknowledgements

This project was supported by the Innovation Program for Graduate Education of Jiangsu Province (KYLX_1063), the Natural Science of Jiangsu Province (BK20141298) and the Society Development Fund of Zhenjiang (SH2013020).

References

1 D. J. Martin, P. J. T. Reardon, Savio J. A. Moniz, J. W. Tang, *J. Am. Chem. Soc.* 2014, **136**, 12568-12571.
2 V. M. D. Rocha, M. D. Pereira, L. R. Teles, M. O. D Souza, *Mater. Sci. Eng. B-Adv*. 2014, **185**, 13-20.
3 M. D. Hernandez-Alonso, F. Fresno, S. Suarez, J. M. Coronado, *Energ. Environ. Sci*. 2009, **2**, 1231-1257.
4 M. Karmaoui, D. M. Tobaldi, A. S. Skapin, R. C. Pullar, M. P. Seabra, J. A. Labrincha, V. S. Amaral, *Rsc. Adv*. 2014, **4**, 46762-46770.
5 S. Z. Hu, L. Ma, J. G. You, F. Y. Li, Z. P. Fan, G. Lu, D. Liu, J. Z. Gui. *Appl. Surf. Sci.* 2014, **311**, 164-171.
6 H. X. Zhao, H. T. Yu, X. Quan, S. Chen, Y. B. Zhang, H. M. Zhao, H. Wang, *Appl. Catal. B-Environ.* 2014, **152**, 46-50.
7 M. Shalom, M. Guttentag, C. Fettkenhauer, S. Inal, D. Neher, A. Llobet, M. Antonietti, *Chem. Mater.* 2014, **26**, 5812-5818.
8 Y. G. Xu, H. Xu, J. Yan, H. M. Li, L. Y. Huang, J. X. Xia, S. Yin, H. M. Shu, *Colloid. Surf. A.* 2013, **436**, 474-483.
9 J. H. Yang, X. T. Wu, X. F. Li, Y. Liu, M. Gao, X. Y. Liu, L. N. Kong, S. Y. Yang, *Appl. Phys. A-Mater.* 2011, **105**, 161-166.
10 Y. G. Li, J. A. Zhang, Q. S. Wang, Y. X. Jin, D. H. Huang, Q. L. Cui, G. T. Zou, *J. Phys. Chem. B.* 2010, **114**, 9429-9434.
11 S. C. Yan, Z. S. Li, Z. G. Zou, *Langmuir* 2009, **25**, 10397-10401.
12 E. G. Gillan, *Chem. Mater.* 2000, **12**, 3906-3912.
13 J. X. Xia, J. Di, S. Yin, H. M. Li, H. Xu, L. Xu, H. M. Shu, M. Q. He, *Mater. Sci. Semicon. Proc.* 2014, **24**, 96-103.
14 A. Thomas, A. Fischer, F. Goettmann, M. Antonietti, J.O. Muller, R. Schlogl, J.M. Carlsson, *J. Mater. Chem*. **2008**, **18**, 4893-4908.
15 J. Chen, S. H. Shen, P. H. Guo, M. Wang, P. Wu, X. X. Wang, L. J. Guo, *Appl. Catal. B-Environ.* 2014, **152**, 335-341.
16 N. Tian, H. W. Huang, Y. He, Y. X. Guo, Y. H. Zhang, *Rsc. Adv*. 2014, **4**, 42716-42722.
17 H. P. Li, J. Y. Liu, W. G. Hou, N. Du, R. J. Zhang, X. T. Tao, *Appl. Catal. B-Environ.* 2014, **160-161**, 89-97.
18 J. Theerthagiri, R. A. Senthil, A. Priya, J. Madhavan, R. J. V. Michael, M. Ashokkumar, *Rsc. Adv*. 2014, **4,** 38222-38229.
19 Z. J. Zhang, W. Z. Wang, L. Wang, S. M. Sun, *ACS Appl. Mater. Inter.* 2012, **4**, 593-597.
20 Y. M. He, J. Cai, T. T. Li, Y. Wu, H. J. Lin, L. H. Zhao, M. F. Luo, *Chem. Eng. J.* 2013, **215**, 721-730.
21 S. Vadivel, V. P. Kamalakannan, *Ceram. Int.* 2014, **40**, 14051–14060.

22 F. Jiang, T. T. Yan, H. Chen, A. W. Sun, C. M. Xu, X. Wang, *Appl. Surf. Sci.* 2014, **295**, 164-172.
23 K. Dai, L. H. Lu, C. H. Liang, Q. Liu, G. P. Zhu, *Appl. Catal. B-Environ.* 2014, **156**, 331-340.
24 X. S. Rong, F. X. Qiu, J. Qin, J. Yan, H. Zhao, D. Y. Yang, *J. Ind. Eng. Chem.* 2014, **20**, 3808-3814.
25 L. Y. Chen, W. D. Zhang, *Appl. Surf. Sci.* 2014, **301**, 428-435.
26 Y. F. Luo, H. Chen, X. Li, Z. Q. Gong, X. J. Wang, X. F. Peng, M. D. He, Z. Z. Sheng, *Mater. Lett.* 2013, **105**, 12-15.
27 Y. M. Cui, Q. F. Jia, H. Q. Li, J. Y. Han, L. J. Zhu, S. G. Li, Y. Zou, J. Yang, *Appl. Surf. Sci.* 2014, **290**, 233-239.
28 L. Y. Huang, H. Xu, R. X. Zhang, X. N. Cheng, J. X. Xia, Y. G. Xu, H. M. Li, *Appl. Surf. Sci.* 2013, **283**, 25-32.
29 H. Katsumata, Y. Tachi, T. Suzuki, S. Kaneco, *Rsc. Adv.* 2014, **4**, 21405-21409.
30 D. S. Wang, H. T. Sun, Q. Z. Luo, X. L. Yang, R. Yin, *Appl. Catal. B-Environ.* 2014, **156**, 323-330.

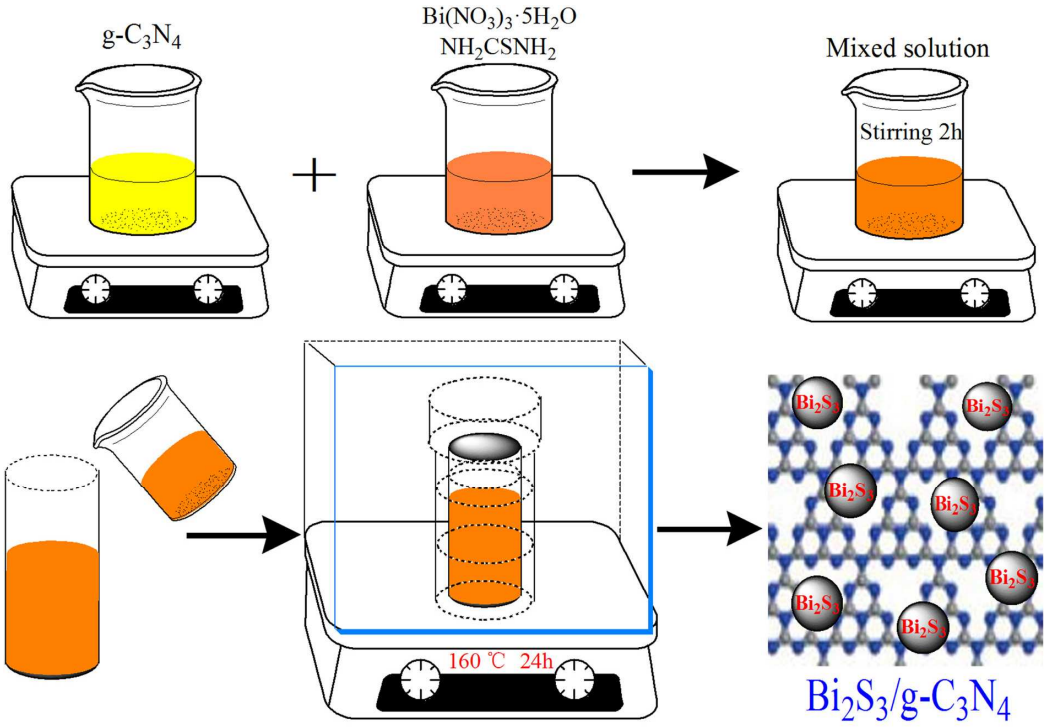

Scheme 1. Preparation process of Bi_2S_3/g-C_3N_4 composite by thermal process

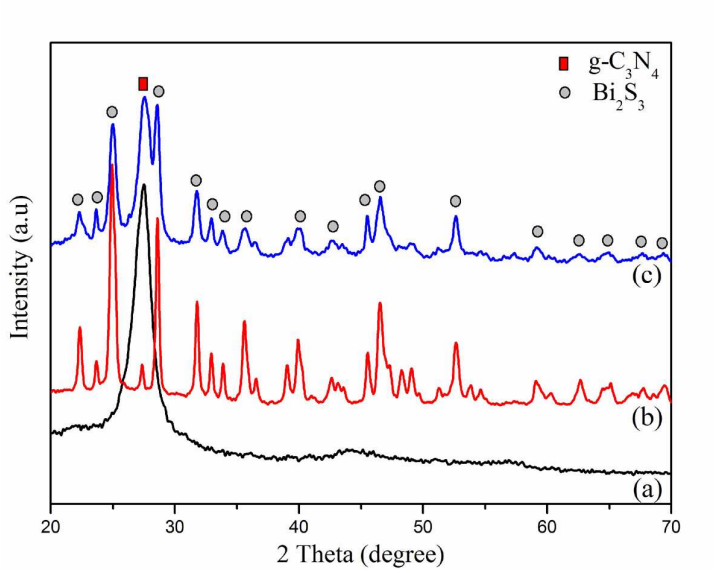

Fig. 1. XRD patterns of g-C_3N_4 (a), Bi_2S_3 (b) and Bi_2S_3/g-C_3N_4-4 (c)

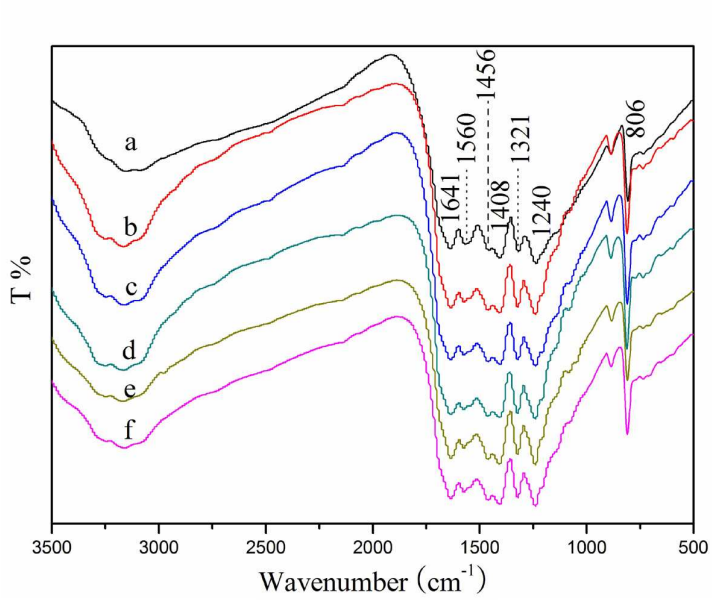

Fig. 2. FT-IR spectra of g-C_3N_4 (a), Bi_2S_3/g-C_3N_4-1 (b), Bi_2S_3/g-C_3N_4-2(c), Bi_2S_3/g-C_3N_4-3 (d), Bi_2S_3/g-C_3N_4-4 (e) and Bi_2S_3/g-C_3N_4-5 (f)

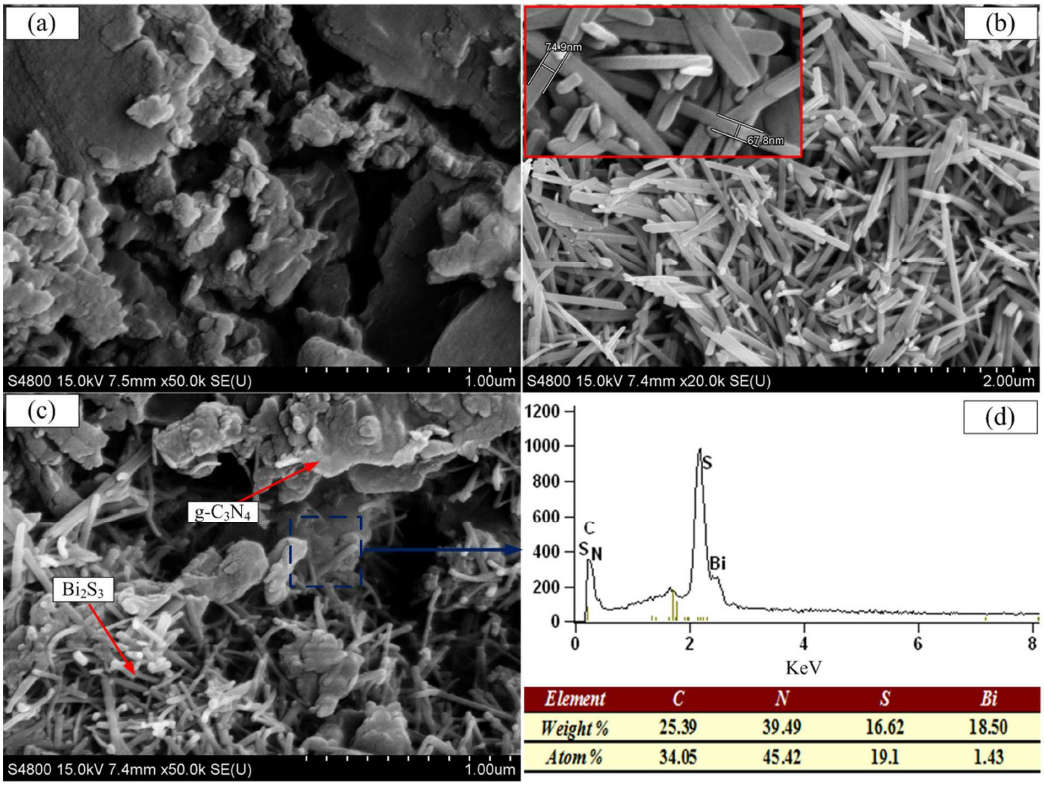

Element	C	N	S	Bi
Weight %	25.39	39.49	16.62	18.50
Atom %	34.05	45.42	19.1	1.43

Fig. 3. SEM images of pure g-C_3N_4 (a), Bi_2S_3 (b) and Bi_2S_3/g-C_3N_4-4 (c) and EDS results (d)

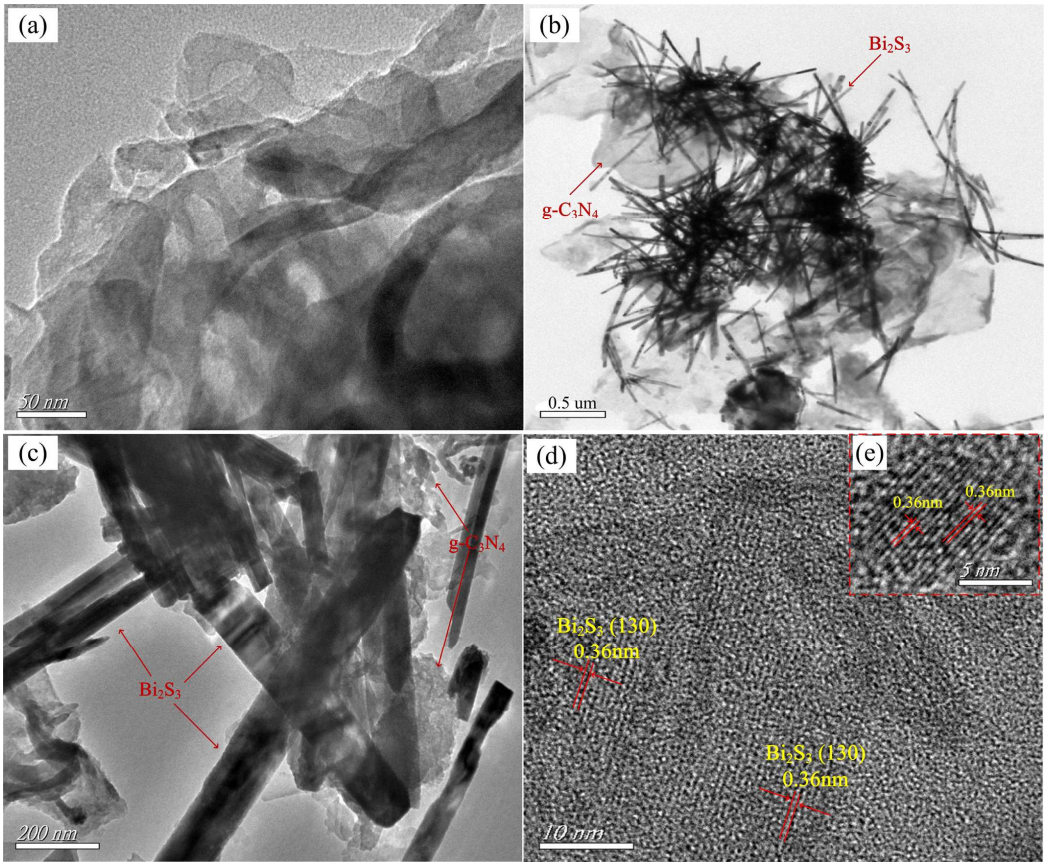

Fig. 4. TEM images of pure $g\text{-}C_3N_4$ (a), $Bi_2S_3/g\text{-}C_3N_4$-4 (b), $Bi_2S_3/g\text{-}C_3N_4$-4 (c) and HRTEM images (d, e) of Bi_2S_3 nanorod

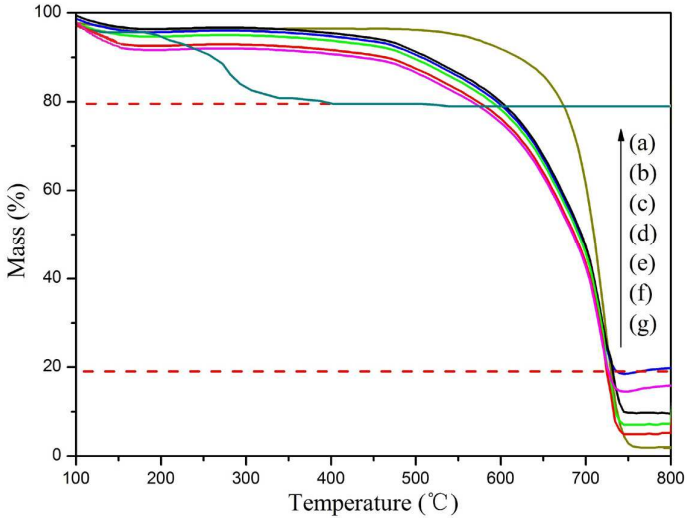

Fig. 5. TG curves of pure Bi_2S_3 (a), Bi_2S_3/g-C_3N_4-5 (b), Bi_2S_3/g-C_3N_4-4 (c), Bi_2S_3/g-C_3N_4-3 (d), Bi_2S_3/g-C_3N_4-2 (e), Bi_2S_3/g-C_3N_4-1 (f) and g-C_3N_4 (g)

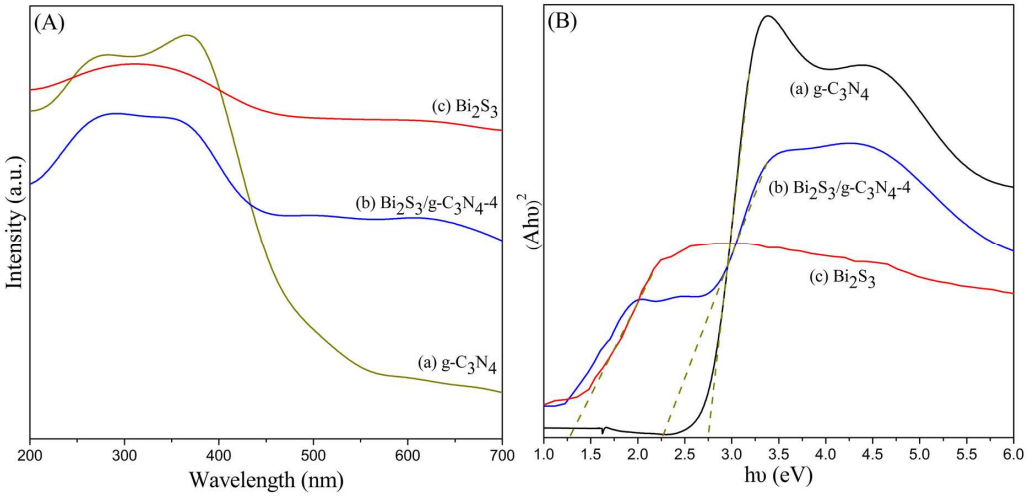

Fig. 6. UV-vis diffuse reflection spectra (DRS) of the pure g-C_3N_4 (a), Bi_2S_3/g-C_3N_4-4 (b) and Bi_2S_3 (c)

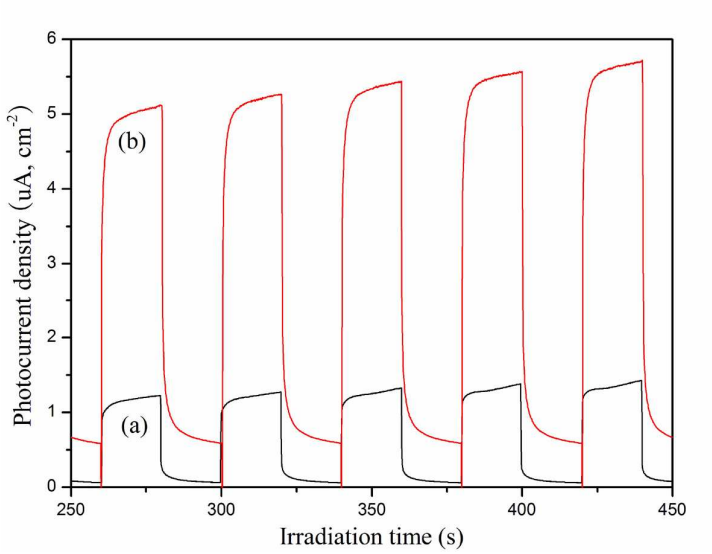

Fig. 7. Transient photocurrent response for the pure g-C_3N_4 (a) and Bi_2S_3/g-C_3N_4-4 (b)

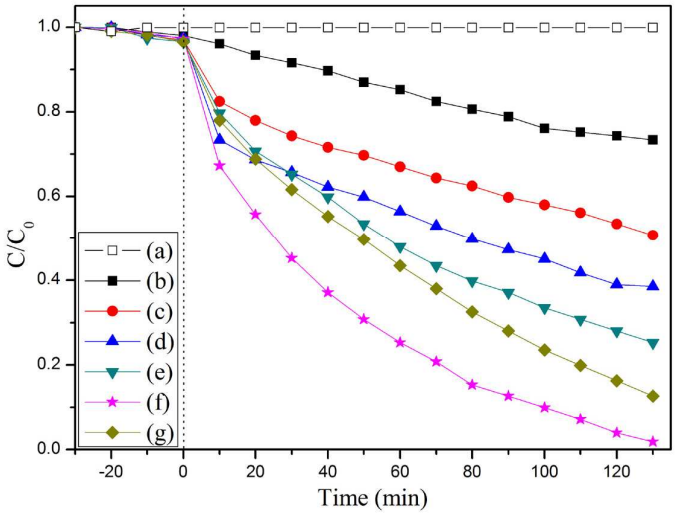

Fig. 8. The photodegradation of RhB for blank experiment (a), g-C_3N_4 (b), Bi_2S_3/g-C_3N_4-1 (c), Bi_2S_3/g-C_3N_4-2 (d), Bi_2S_3/g-C_3N_4-3 (e), Bi_2S_3/g-C_3N_4-4 (f) and Bi_2S_3/g-C_3N_4-5 (g) samples

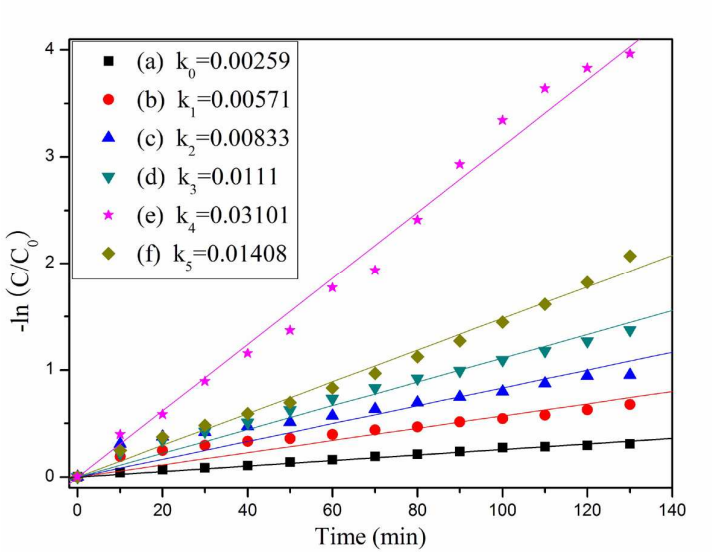

Fig. 9. The first-order kinetics of RhB degradation in the presence of g-C_3N_4 (a), Bi_2S_3/g-C_3N_4-1 (b), Bi_2S_3/g-C_3N_4-2 (c), Bi_2S_3/g-C_3N_4-3 (d), Bi_2S_3/g-C_3N_4-4 (e) and Bi_2S_3/g-C_3N_4-5 (f) samples

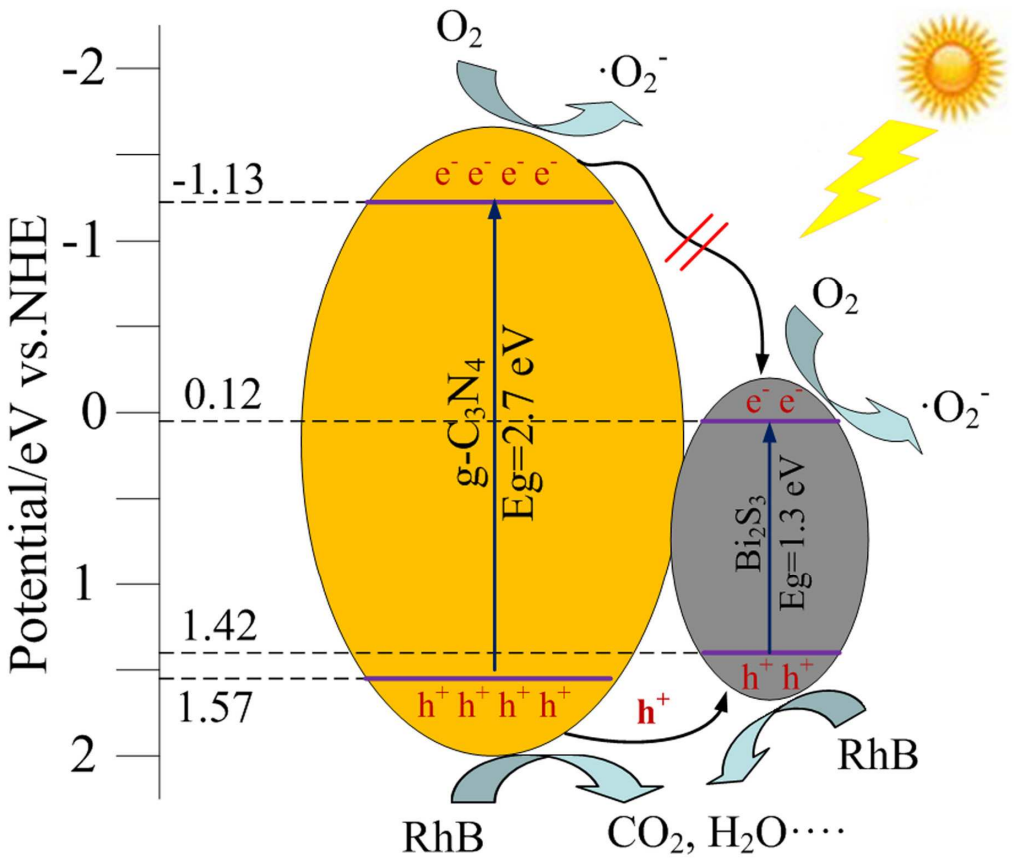

Scheme 2. Schematic diagram of the separation and transfer of photogenerated charges in the Bi_2S_3/g-C_3N_4 photocatalyst under visible light irradiation

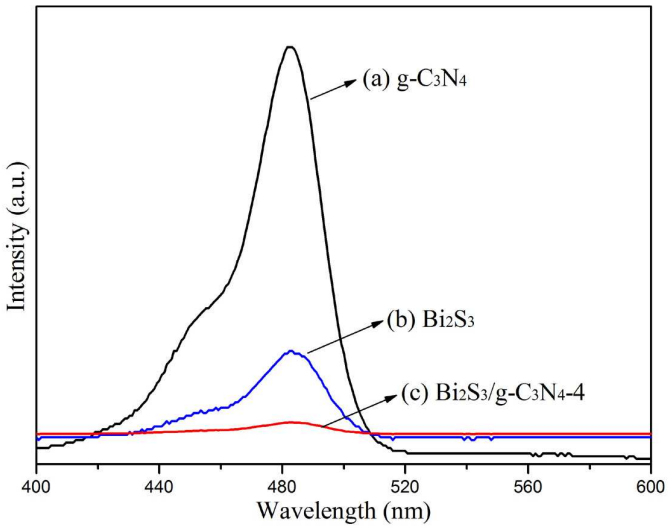

Fig. 10. PL spectra of pure g-C_3N_4 (a), Bi_2S_3 (b) and Bi_2S_3/g-C_3N_4-4 (c)

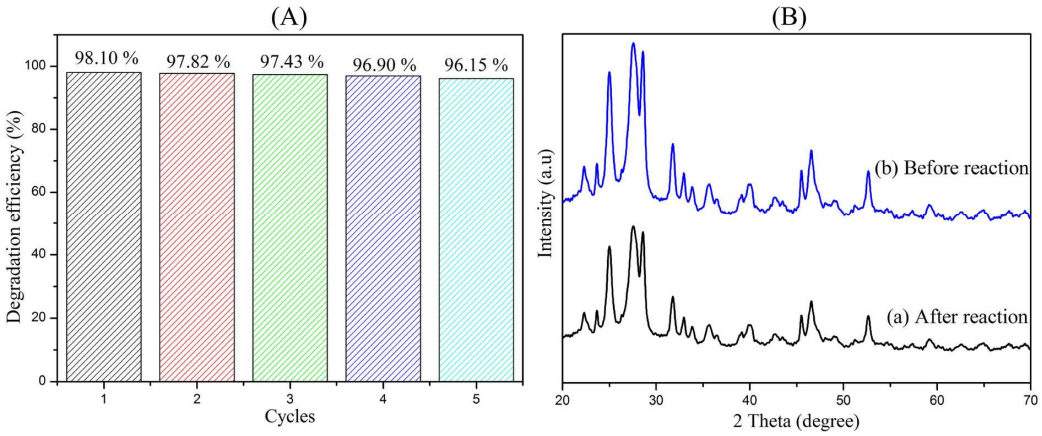

Fig. 11. Reuse experiments of the Bi_2S_3/g-C_3N_4-4 in the photodegradation of RhB under visible light irradiation (A), and the XRD patterns of Bi_2S_3/g-C_3N_4-4 before and after photocatalytic reaction (B)